AEB effective evaluations by accident reconstructions using videos of drive recorders in perpendicular and turning car-to-cyclist collisions

Yuqing Zhao, Daisuke Ito, Koji Mizuno, Chunyu Kong

Abstract A drive recorder provides useful information to analyze factors that caused accidents. The information includes the driving video, car velocity, acceleration data, brake/turning indicator data, and GPS data. In this research, 237 videos of accidents involving taxi-to-cyclist collisions at intersections were collected from drive recorders. The collision data were compared to near-miss incident data to identify the factors that made the difference between collisions and near-miss incidents. It was shown that collisions occurred when cyclists entered an area where a car deceleration over 0.55 *G* was necessary to stop the car from colliding with the cyclist. In left and right turn collisions, the car velocity was low and many drivers had already braked when entering the intersection. Therefore, the cause of the accident was likely related to the driver's perception. To investigate the effectiveness of autonomous emergency braking (AEB) systems, car-to-cyclist collisions were reconstructed using PC-Crash simulations that were based on the videos from the drive recorders. Extending the field of view (FOV) of AEB system from 50° to 90° was effective in reducing the number of collisions in perpendicular and left- and right-turn collisions. With an ideal AEB with a 360° FOV and no sensor delay time, 52 of the 63 perpendicular collisions and 49 of 51 left and right turn collisions were avoidable.

Keywords Crash avoidance, Autonomous emergency braking, Car-cyclist collision, Accident reconstruction

I. INTRODUCTION

Protecting vulnerable road users in traffic accidents is one of the world's largest health issues. In Japan, pedestrians and cyclists accounted for 31.7% and 11.8%, respectively, of the 3,694 traffic fatalities in 2017. It is well known that the injury risk to a pedestrian in car-to-pedestrian collisions decreases sharply with a decrease in impact velocity [1,2]. Therefore, if the use of autonomous emergency braking (AEB) systems that detect pedestrians and cyclists can avoid collisions or reduce impact velocities, substantial benefits can be obtained from the decrease in the number of victims in car-to-pedestrian and car-to-cyclist collisions.

The effectiveness of AEB in pedestrian collisions has been investigated by estimating the number of injuries which could have benefited from an AEB using in-depth accident data. Rosén [3,4] calculated the effectiveness of AEB with changing parameters using the GIDAS database, and found that AEB systems having sensors with a field of view (FOV) of 40° and providing a braking deceleration of 0.6 *G* were 40% effective in preventing fatalities. Since high-velocity impacts occur within a small angle FOV, most fatally or seriously injured pedestrians were contained in a 40° FOV in one second before impact. Páez et al. [5] reconstructed 50 car-to-pedestrian collisions that occurred in Madrid using PC-Crash, and recalculated the selected cases in PC-Crash after implementing an AEB system. Their results showed that 42% of the car-to-pedestrian collisions could be avoidable with AEB.

Since cyclists have a traveling velocity, AEB sensors are required to perform more robustly in cyclist collision avoidance than in pedestrian collision scenarios. Fredriksson et al. [6] applied the same method of car-to-pedestrian collisions to car-to-cyclist collisions in AEB effectiveness calculation, and estimated that an AEB system with a larger FOV could reduce more AIS3+ head injuries to cyclists. Op den Camp et al. [7] and Lenard et al. [8] analyzed the cyclists' behavior before collisions, and found that cyclists had a wider distribution of their locations relative to the car compared to pedestrians. Furthermore, they indicated that AEB sensors for cyclists need to cover a 180° range. On the other hand, some research studies indicate that AEB is equally effective for pedestrian and cyclist injuries. Barrow et al. [9] simulated the AEB system for in-depth accident data of pedestrians and

Yuqing Zhao is a MEng student in Mechanical Systems Engineering at Nagoya University in Japan (zhao.yuqing@b.mbox.nagoya-u.ac.jp). Daisuke Ito and Koji Mizuno are Assistant Professor and Professor in the Department of Mechanical Systems Engineering at Nagoya University in Japan. Chunyu Kong is Associate Professor in the School of Automobile and Transportation Engineering at Guangdong Polytechnic Normal University in China.

cyclists, with a sensor FOV 60°, and found that the effectiveness for reduction of fatal and serious injuries to pedestrians (58.7%) and cyclists (53.1%) was comparable. Using GIDAS PCM data, Rosén (2013) calculated the effectiveness of pedestrian and of cyclist fatalities to be 80% for advanced AEB (FOV 90°) and 50% for reference AEB (FOV 40°).

Many studies calculated the benefit of AEB using in-depth data. In analyzing the in-depth accident data, the pedestrian and cyclist trajectories before collisions were determined based on the testimony of accident involved persons and of witnesses or by using statistical velocity distributions as a function of age [3]. The car impact velocity was determined from tire skid marks, car deformations, and the pedestrians' and cyclists' fall distances. Accordingly, in-depth accident data can include uncertainness of pedestrian, cyclist behavior and car velocity in the pre-crash phase [4]. Meanwhile, pedestrian behavior and road obstructions can be observed in the videos of drive recorder camera, and have the potential to explain factors which led to collisions [10]. Han et al. [11] classified the pedestrian behavior before/during/after impact using videos, which otherwise was difficult to determine without such videos. From the videos of the drive recorders, Ito et al. [12] showed cyclists took collision avoidance actions such as decelerating, accelerating, steering, and lifting of their struck side leg in collisions. The database of near-miss incidents of drive recorder videos also provides information of pedestrian or cyclist behavior [13,14]. Nevertheless, the data of near-miss incidents are difficult to use for determining AEB effectiveness since collisions did not occur in the near-miss incidents. As far as authors' knowledge, there are few studies that AEB effectiveness has been calculated using drive recorder videos of collisions.

In our previous studies [12, 15], the occurrence factors of car-cyclist perpendicular collisions were investigated using the videos of drive recorders. The collisions were reconstructed by PC-Crash and the recalculated after having implemented a virtual AEB into the car model. On the other hand, the number of injuries in perpendicular collisions and left and right turn collisions are comparable with each other [16, 17]. However, few research studies compared the effectiveness of AEB for individual car-to-cyclist collision configurations. In this paper, occurrence factors and AEB effectiveness of car in turning collisions were also examined while changing the AEB parameters. This study was approved by the Ethics Committee in the Graduate School of Engineering in Nagoya University (No. 17-13).

II. METHODS

Database

In this study, the accident data of drive recorders were provided by taxi companies in Aichi prefecture with the help of the Aichi Taxi Association and Nagoya Taxi Association. The data were collected from the collisions of taxis without AEB. Containing data for car-to-car, car-to-pedestrian and car-to-cyclist collisions, the total number of cases collected was 1,163 in 2018. The near-miss incident database of drive recorders from Tokyo University of Agriculture and Technology was used to compare collisions. The drive recorder data include vehicle velocity, acceleration data, braking data, turning indicator data, and GPS information.

In this study, two types of collisions which had occurred in intersections were examined. The first type was perpendicular collisions at an intersection as shown in Fig. 1(a): a car traveling straight hit a cyclist who came from

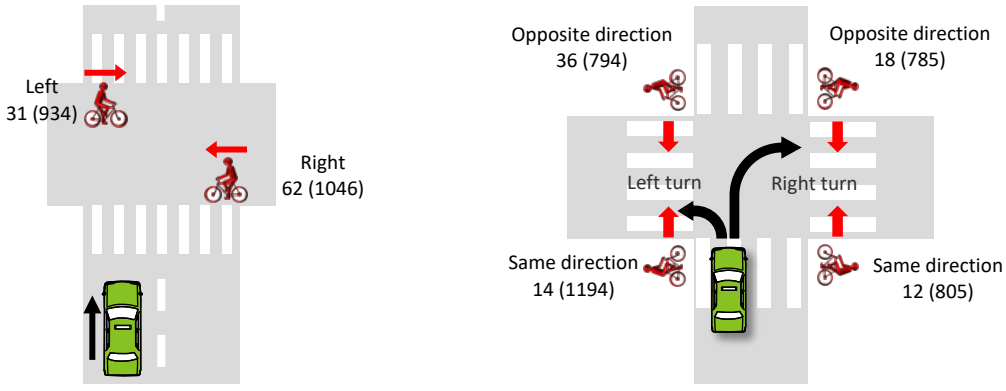

(a) Perpendicular collision (b) Left and right turn collision

Fig. 1. Definition of car-to-cyclist collision types. The figures show the number of collisions (near-miss incidents).

the left or right side. The second type was left and right turn collisions as shown in Fig. 1(b): a car turning left or right collides with a cyclist who traveled from the opposite or the same direction of the car's direction. Note in Japan, cars and cyclists should travel on the left side of roads, while cyclists are allowed to travel in either side of streets having wide pavements. If the cyclist was crossing before the car started to turn (which can be judged from the turning indicators), the collision configuration was not included in this study. Near-miss data (2005-2016) includes approximately 10,523 car-to-cyclist incidents, and were screened to obtain a smaller sample for this study [13]. The number of collected car-to-cyclist collisions at intersection was 237, including 93 perpendicular collisions, 50 left turn and 30 right turn collisions, and 64 "other" collisions. Among these, 27 perpendicular, and 9 left and 6 right turn collision data were extracted from the near-miss incidents database.

Video Analysis

From video analysis, after removing distortions toward the corner of the image, the horizon line and the vanishing point of view were obtained; and the perspective transformation was applied to the image. Then, the transformation coefficient was calculated based on the length of fixed objects present in the video such as a crosswalk on the road.

The characteristic time from the time of the collision was defined as follows:

- t_A: the time of the cyclist appearing from the obstacle. If the cyclist did not appear behind obstacles in the video, t_A was estimated based on obstacle locations identified in Google map.
- t_B: the time of the driver pushing the brake pedal (judged by brake lights) to stop the car to avoid the collision against the cyclist.
- t_E: the time of the cyclist entering the intersection from the pavement.

Basically, the accident can be reconstructed from t_A to investigate the effect of obstacles appearing in the driver view. Assuming the cyclist traveled at a constant velocity before time t_A, at least 5 seconds before collisions were examined in the accident analysis.

TTC in Perpendicular Collisions and Left and Right Turn Collisions

In accident analysis, the time-to-collision (TTC) was obtained using the remaining time of the car before collision as shown in the video. In near crashes, actual crashes did not occur, therefore, the point of crash was defined as the point where a potential collision would occur if the driver or the cyclist took no actions and traveled along the original path.

In accident reconstructions with an installed AEB, it was assumed the collision point before collision was unknown, and the TTC was calculated based on distance and velocity for braking start. In car-to-cyclist perpendicular collisions (Fig. 2(a)), TTC is determined by the distance from the car to the collision point D and car velocity V as follows:

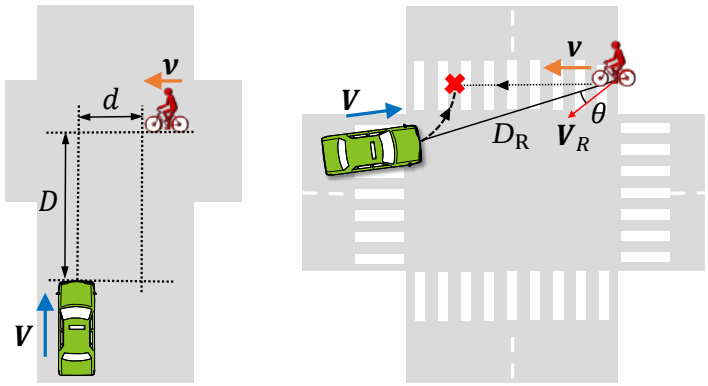

(a) Perpendicular collision (b) Left turn collision

Fig. 2. Relative distance and velocity between car and cyclist.

$$TTC = D/V \tag{1}$$

Assuming the car has a constant deceleration a_0, the velocity V and the distance D of the car can be expressed as:

$$0^2 - V^2 = 2(-a_0)D \tag{2}$$

From Eqs. (1) and (2), TTC can be expressed by:

$$V = 2 \cdot a_0 \cdot TTC \tag{3}$$

When the deceleration is at the maximum value a_{max}, TTC becomes the time limit in which the car can stop safely. If the required deceleration exceeds the actual braking limit of the car, the car cannot stop in time to avoid the collision.

In left and right turn collisions (Fig. 2(b)), the relative velocity vector of cyclist with respect to the car $\boldsymbol{V}_R$ is calculated by car velocity $\boldsymbol{V}$ and cyclist velocity $\boldsymbol{v}$ as:

$$\boldsymbol{V}_R = \boldsymbol{v} - \boldsymbol{V} \tag{4}$$

Assuming $\boldsymbol{V}_R$ forms an angle θ relative to the car-to-cyclist direction, the effective velocity of the cyclist closing in on the car is $V_R \cdot \cos\theta$ (V_R: the magnitude of $\boldsymbol{V}_R$). Accordingly, TTC in left and right turn collisions can be calculated by using the effective closing velocity of cyclist with respect to the car as follows:

$$TTC = \frac{D_R}{V_R \cdot \cos\theta} \tag{5}$$

where D_R is the distance between the car and the cyclist.

Reconstruction and AEB Algorithm

The collision site was determined by the longitude and latitude GPS coordinates based on the map information of the drive recorder data. The 3D Google map was employed to determine the obstacle and the surrounding environment of the accident; and the aerial photograph of the street where the accident occurred was scaled according to the map information after being imported into PC-Crash. The contact time of the car and the cyclist was defined as time 0; and this was taken to be the reference time of the reconstruction. The trajectory of the car was determined backwards from the reference time based on the car velocity, acceleration and distance that were obtained from drive recorder data and video. The cyclist position was decided from the video. In the case where a cyclist was not shown continuously due to obstacles, the cyclist was assumed to move at a constant velocity.

Perpendicular and left and right turn collisions for which the occurrence site could be identified were reconstructed using PC-Crash Ver. 11.1. The accident reconstruction was calculated again using a car model with AEB installed. FOV of virtual AEB was divided into three different types as shown in Fig. 3. The first was a FOV of 50° (±25°) with a detection distance of 50 m, which was used for pedestrian detection [18]. The second was an AEB sensor with a FOV of 90° (±45°) with a detection distance of 75 m. This FOV was set to be able to find the cyclist target from its starting point in car-to-cyclist near side scenario in Euro NCAP AEB tests [19]. The third type of AEB was set to be an ideal AEB where the FOV was 360° with a detection distance of 75 m. This allowed obstacles in the entire circumference to be detected.

Sensor detection delay time (SDT) was the time from which the cyclist entered the sensing area to the time that the cyclist was detected. Brake pre-charge time (BPT) was time taken for the brake pads to contact the brake disc. The sum of SDT and BPT was referred to as Delay Time (DT). The Brake Boosting Time (BBT) referred to the time taken to reach maximum deceleration. SDT and BPT were set to 0.4 s and 0.1 s, respectively [20]; and BBT was set to 0.15 s. Fig. 4 shows the AEB time series from the time when the cyclist enters into the field of view (t_{FOV}) until AEB ends. It is possible to recognize a cyclist who enters into the sensing area and calculate TTC after SDT. When TTC is less than 1.4 s, deceleration starts after BPT, increasing from 0 to a maximum deceleration of 0.8 *G* during BBT, and remains at a maximum deceleration of 0.8 *G* until the car stops.

Delay time was set to 0 s in the ideal AEB, meaning that the cyclist can be detected immediately once it entered the FOV. This 0 s delay time showed the upper limit of the AEB performance. Note that cyclists who traveled on the pavement were not judged as a hazard, even though they were included in the sensor's FOV. Once cyclists began to enter the road from the pavement, the algorithm then judged whether they collided with the car. Hence, this time (t_E) was used for the trigger of AEB activation.

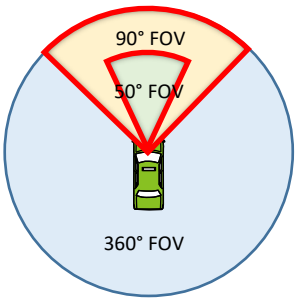

Fig. 3. Three types of AEB sensor FOVs.

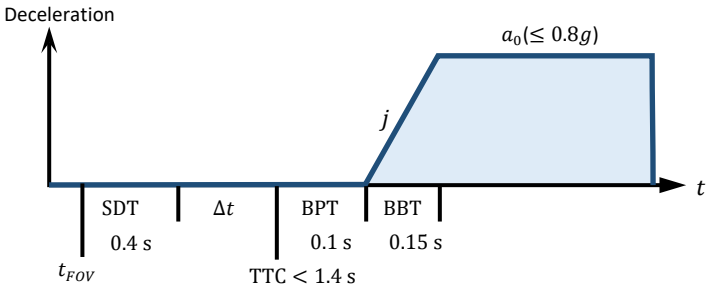

Fig. 4. Vehicle deceleration versus AEB activation with time.

III. RESULTS

Accident Analysis

(1) Car velocity

Car velocity distributions at time at cyclists' appearance t_A, and at the time of collision are plotted in Fig. 5. Among crash configurations, the car velocities at cyclist appearance are in the order of those of the perpendicular collisions, right turn and left turn collisions. This is because cars reduce velocities in turning, especially for left turns with a small radius of rotation. Comparing Fig. 5(a) and (b), the car velocity decreases from time of cyclist appearance to that of collision in perpendicular collisions. In right and left turn collisions, there is not a clear tendency of car velocity reduction.

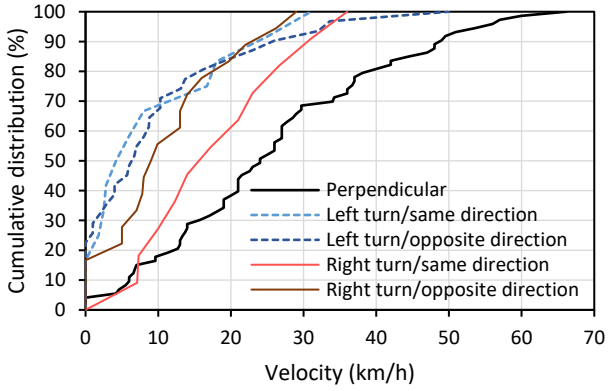

(a) Time at cyclist appearance t_A

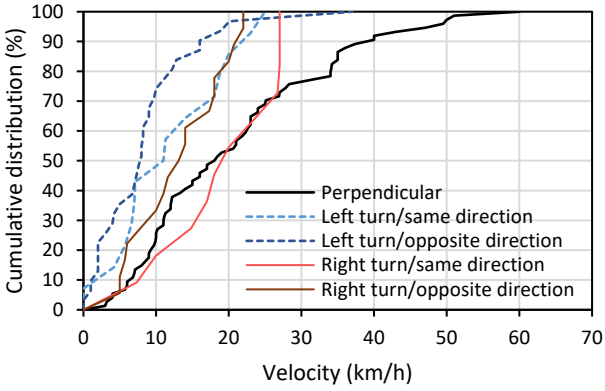

(b) Time at collision

Fig. 5. Car velocity distributions

(2) Sight obstructions

Fig. 6 shows obstructions which affected the drivers' view as observed when analyzing the videos. The fixed objects include building, house, wall and vegetation. A case where cyclist appeared in the video without an obstruction was classified as "no obstruction". Pedestrian and cyclist can be a sight obstruction from drivers. In perpendicular collisions, the percentage of fixed objects occupies more than 50% of the cases. This is likely because many perpendicular collisions occur in small roads without signals [12]. In these narrow intersections, the fixed objects are built frequently at roadsides. The percentage of obstructions in collisions is larger than that in the near-miss data, suggesting that sight obstructions can be one of the causes of collisions.

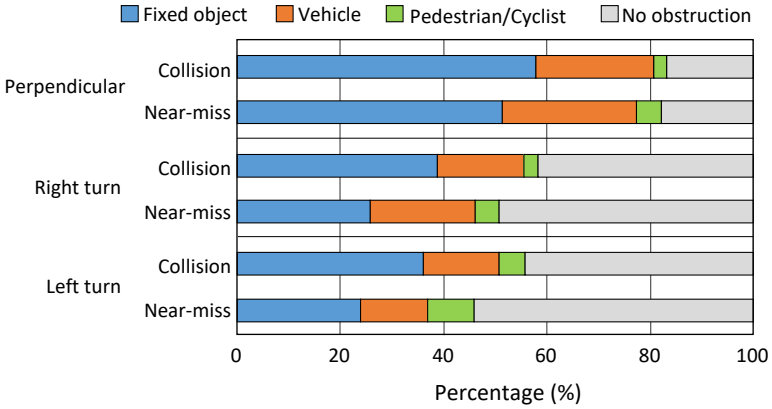

Fig. 6. Sight obstructions for drivers to find cyclists.

(3) Cyclist trajectory

Fig. 7 shows the relative trajectories of cyclists in perpendicular collisions. The areas are FOV 50° and 90° from the car, respectively. The different colors of the trajectory lines represent the different car velocities at the time of the cyclist's appearance (t_A). There were cases where car velocities of over 60 km/h were near the center of the FOV area. Though the trajectories of most of the cyclists were within the 90° FOV, there were cases where the car trajectories were outside the 90° FOV area. This suggests that expanding the AEB sensing area is effective for car-to-cyclist collisions.

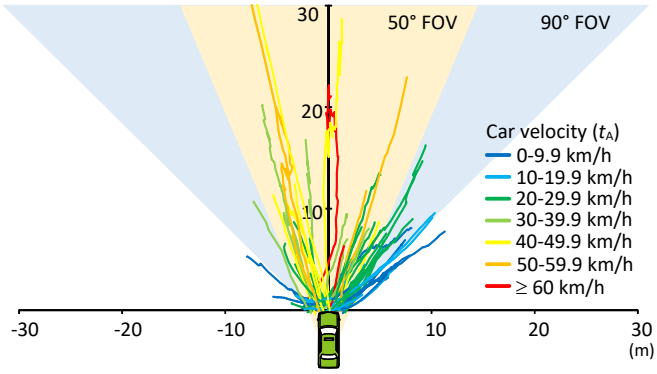

Fig. 7. Trajectories of cyclists relative to the car in perpendicular collisions (near-miss data are not included).

Fig. 8 shows the relative trajectory of the left and right turn collisions. The circle on the trajectory line was the relative position of the cyclist at t_E. In the collision where the cyclist appeared from the same direction as the car's direction (Fig. 8(a) and (c)), all the relative trajectories were in the car-turning side from the car's view. In these collisions, most of the cyclists were outside the 90° FOV, which suggests a large FOV of AEB sensor will be necessary. On the other hand, in the cases where the cyclist appeared from the opposite direction (Fig. 8(b) & (d)), cyclist trajectories were presented for both the left and right sides. In these cases, cyclists approached from the front of the car, and most of the cyclists were included inside the FOV 90° area. Compared to perpendicular collisions, car velocities in right and left turning collisions were lower, and most of them were less than 20 km/h at t_E.

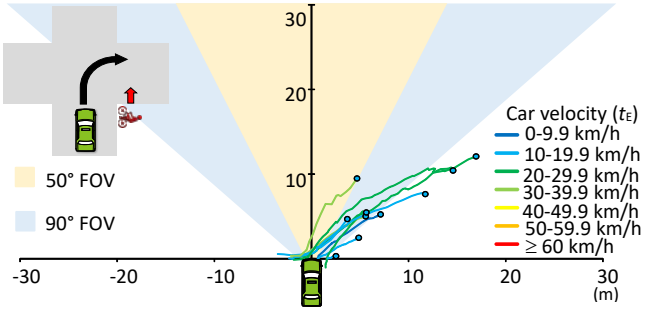

(a) Right turn and cyclist same direction

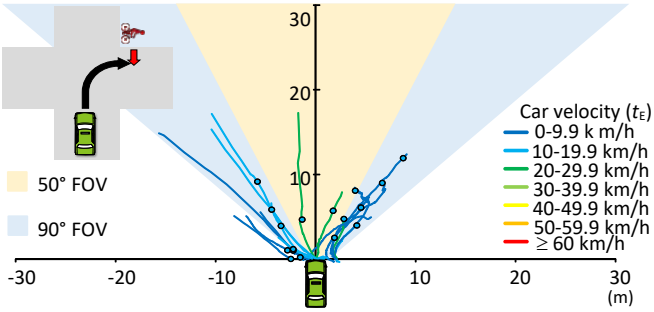

(b) Right turn and cyclist opposite direction

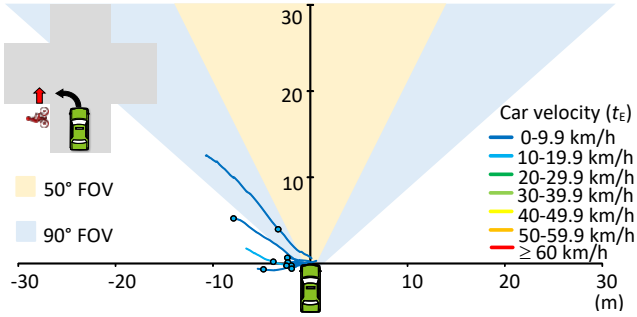

(c) Left turn and cyclist same direction

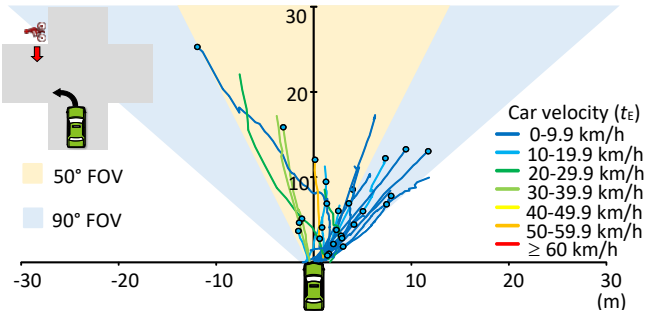

(d) Left turn and cyclist opposite direction

Fig. 8. Trajectories of cyclists relative to the car in left and right turn collisions (near-miss data are not included). The circles show the position where cyclists entered the road from the pavement.

(4) TTC and car velocity

The probability $P(x)$ of perpendicular accident occurrence was calculated as a function of car deceleration ($= V_B/(2\,TTC_B)$). P=0 is near-miss incidents of only car avoided case, and P=1 is a collision. In survival analysis using Weibull function, the probability was calculated as:

$$P(x) = 1 - \exp\left(-\frac{x}{5.668}\right)^{9.487} \quad (6)$$

Based on the above curve, the car deceleration 0.55 *G* corresponds with 50% probability of collision occurrence (Fig. 9). As the car deceleration exceeds 0.7 *G*, the probability of collision occurrence is close to 100%.

For collisions and near-miss incidents in perpendicular cases, the relationship between the car velocity V_B and the TTC_B at the time t_B when the driver starts braking is shown in Fig. 10. Near-miss incident data also are distributed in the area where the acceleration of 0.55 *G* or more is needed for cars to stop. This is because the near-miss incidents did not result in a collision when either the car, or the cyclist, or both of them avoided the collision. However, since the focus was on the driver's behavior in this research, only cases where the car avoided the collision were examined. In the figure, the line shows the maximum deceleration of 0.55 *G* without braking delay time to avoid a collision. Collisions and near-miss incidents (only car avoided) can be separated by the line (0.55 *G*), excluding collisions with a low velocity of V_B less than 15 km/h. This result indicates that collisions occurred when cars needed to stop with a deceleration of more than 0.55 *G* to avoid the collision when the cyclist did not take actions to avoid the collision.

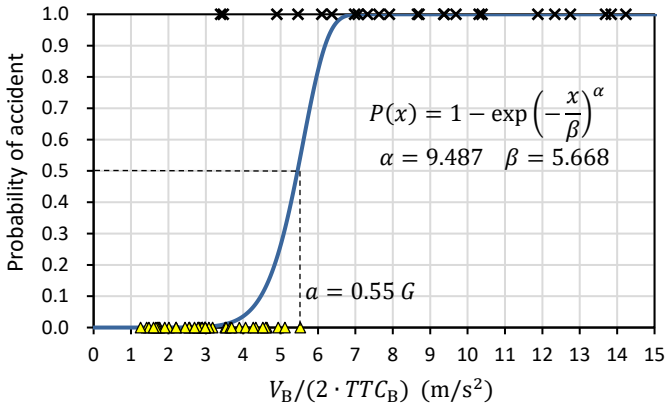

Fig. 9 Probability of accidents as a function of vehicle deceleration (V_B>15 km/h)

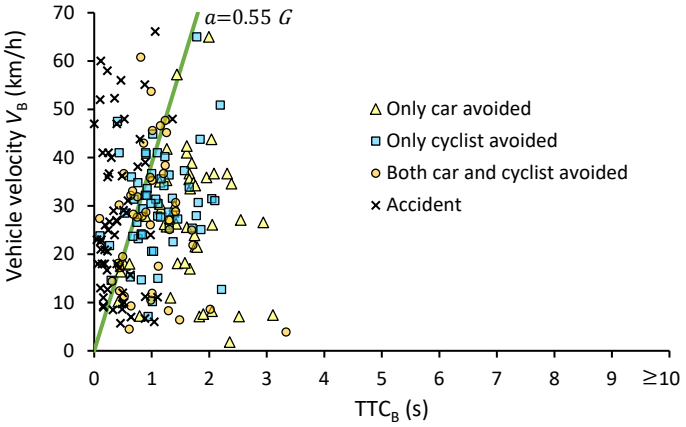

Fig. 10 Relationship between TTC_B and car velocity V_B at t_B in perpendicular collisions.

In left and right turn collisions, many drivers braked before/during the time when the car was turning, and the start time of braking to avoid the collisions cannot be identified. Thus, the relationship between the car velocity V_E and the TTC_E at the time t_E when the cyclist entered the road from the pavement was examined (Fig. 11). Irrespective of car and cyclist directions, the car velocity was low, TTC was long, and collision data were outside of the maximum deceleration area. Hence, collisions could be avoided if the drivers noticed the cyclists and took avoidance maneuvers during left or right turns.

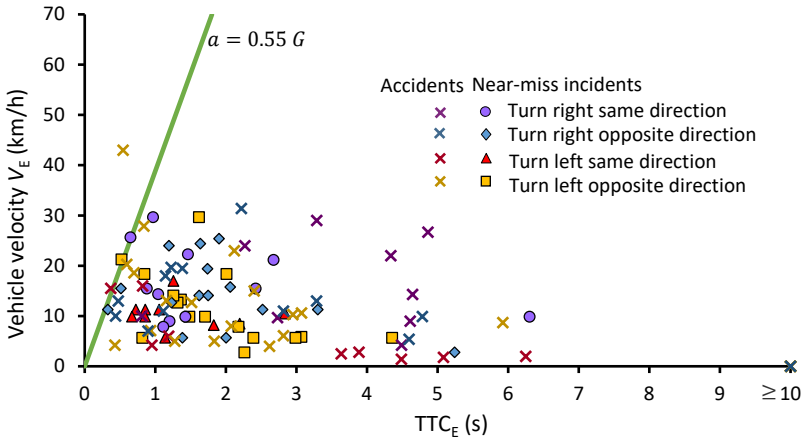

Fig. 11. Relationship between TTC_E and car velocity V_E when cyclists enter the intersection in left and right turn crash configurations.

AEB Effectiveness Analysis

(1) Perpendicular collisions

Sixty-three (63) perpendicular collisions were reconstructed. Fig. 12 shows two examples of collision reconstructions with an installed virtual AEB where the FOV is 50° and the DT is 0.5 s. Case1 was a perpendicular collision without any obstruction. The velocity of the car and the cyclist was 48.4 km/h and 22.8 km/h, respectively, at the time of cyclist appearance (t_A); and 51 km/h and 12 km/h, respectively, at the time of collision. In the reconstruction with AEB, the cyclist was continuously present in the FOV of AEB; therefore, the car could stop to avoid a collision. Case2 was an accident where a car collided into a cyclist traveling on the pedestrian crosswalk at an intersection. The velocity of the car and the cyclist was 24.3 km/h and 15 km/h, respectively, at t_A; and 12 km/h and 15 km/h, respectively, at the time of collision. In the reconstruction with the installed AEB, since the car velocity was low, the angle of the cyclist relative to the car remained almost constant; and as a result the cyclist was continuously located outside the FOV of AEB. Therefore, the AEB did not work and the collision occurred.

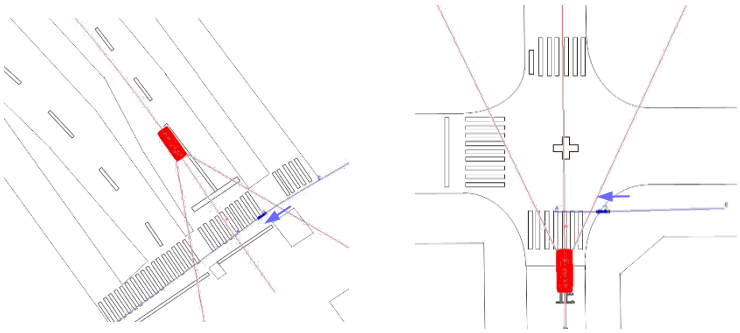

(a) Case1 (b) Case2

Fig. 12. Reconstructions of cars with AEB systems installed in perpendicular collisions: Collision avoided (Case1) and not avoided (Case2).

Fig. 13 shows the relationship between TTC_A and car velocity at t_A with different FOV angles and a constant DT of 0.5 s. The sensor angle greatly affected collision avoidance. Among the 63 collisions, only 14 collisions were avoided with a FOV angle of 50°. In these collisions, the car velocity V was relatively high compared to the cyclist velocity v; and the angle θ of the cyclist position from the car was small ($\tan\theta = v/V$). Hence, the cyclist could be detected with small angle of FOV (e.g. Fig. 12(a)). Eighteen (18) more collisions were avoided by extending the FOV angle to 90°. A further 8 collisions were avoided by extending the FOV angle to 360°. In 15 collisions with the FOV angle of 360°, the cars decelerated due to the AEB system, but still collided with the cyclist. The AEB was not activated for the remaining 8 collisions even at the comprehensive angle of 360°. This is because the car collided with the cyclist before the vehicle started deceleration due to the braking delay time DT (0.5 s).

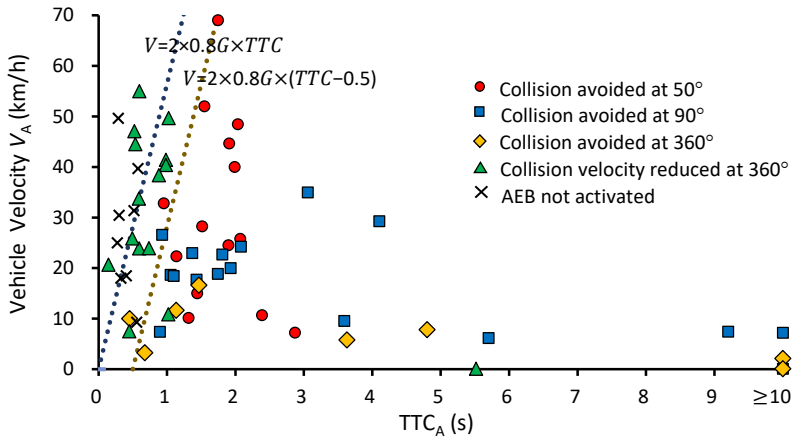

Fig. 13. Collision avoidance with TTC and vehicle velocity at t_A for various FOV and DT 0.5 s in perpendicular collisions. [The dotted lines show Eq. (2) substituting the deceleration 0.8 *G* and the DT 0.0 and 0.5 s (BBT was omitted for simplicity in these lines).]

The position of the cyclist relative to the car at t_A is shown in Fig. 14 for FOV angles of 50°, 90°, and 360°. Sixteen (16) cyclists appeared in the FOV 50°, and 24 more cyclists were in the 90° FOV area. The remaining 23 cyclists were outside of the FOV 90° area. Seven (7) cyclists were outside of the 90° FOV area; and the collisions were avoided since they were included in the 90° FOV area during their approach to the car. There were 5 cyclists included in the 90° FOV area for which the collisions were not avoided. These collisions occurred because the

cyclists appeared suddenly within about 10 m in the *xy* (i.e., longitude and latitude) coordinates in front of the car at t_A.

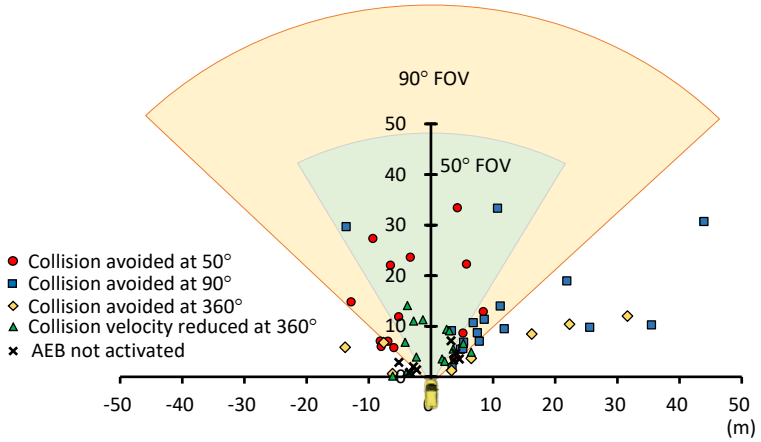

Fig. 14. Cyclist position relative to car at t_A with collision avoidance for various AEB FOVs and DT 0.5 s in perpendicular collisions.

Fig. 15 shows the ratio of AEB effectiveness from the three different virtual AEB systems using 63 reconstructed perpendicular cases. Using the sensor with 50° FOV and 50 m of distance, 22.2% of the collisions were avoided, and AEB was not activated in 58.7% of the cases. This indicates that the FOV for pedestrian AEB is not enough to avoid cyclist collisions. The effectiveness of AEB can be increased by enlarging the angle of the sensor's FOV to 90°. In this case, the ratio of collision avoidance reaches 50.8%, and 22.2% of velocity reduction with activated AEB. Nonetheless, there were still 27% of the reconstructed collisions where the cyclist did not enter the sensing area, and AEB did not work. With an ideal AEB sensor of 360° and DT of 0 s, a significant 82.5% of the collisions can be avoided. However, 17.5% of the collisions (11 cases) still cannot be avoided even using this ideal AEB because the cyclists appear suddenly and the TTC was less than 0.9 s.

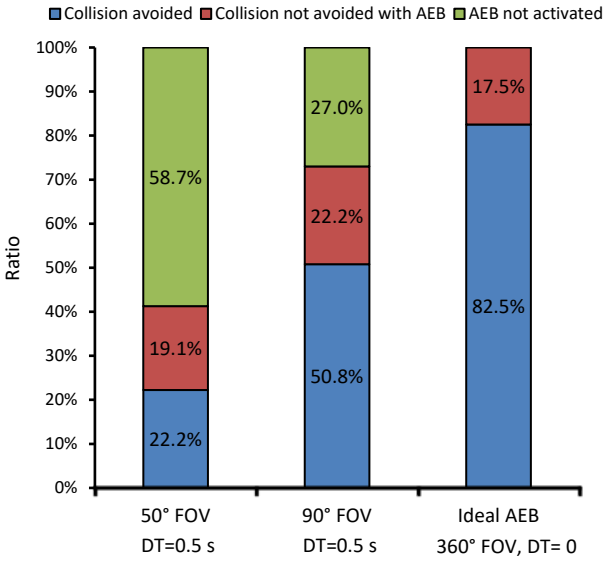

Fig. 15. The ratio of AEB effectiveness in avoiding collisions in perpendicular collisions (N=63).

(2) Left and right turn collisions

Fifty-one (51) left and right turn collisions were reconstructed and divided into 19 cases of right turn collisions and 32 cases of left turn collisions. Fig. 16 shows two examples of reconstructions with AEB in left and right turn collision where the sensor angle is 50° and the DT is 0.5 s. Case3 was an accident where the car turned right and the cyclist appeared from the opposite direction. The velocity of the car and the cyclist was 12.7 km/h and 10 km/h, respectively, at t_E; and 17 km/h and 10 km/h, respectively, at the time of collision. In the reconstruction with AEB, since the cyclist traveled from the opposite direction of the car and was continuously located in the front view of the car, the AEB activated and the collision could be avoided. In Case4, the car turned left and the cyclist traveled from the same direction. The velocity of the car and the cyclist

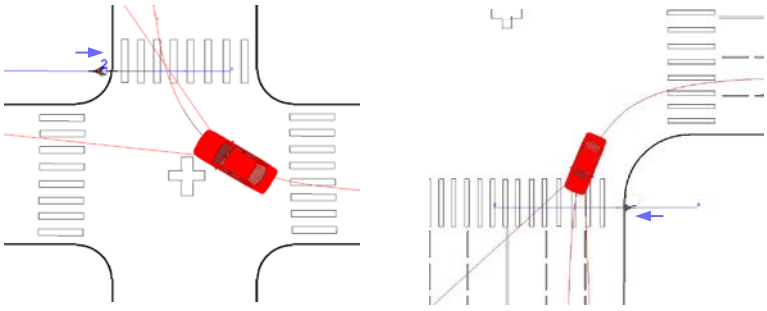

(a) Case3 (b) Case4

Fig. 16. Reconstructions with AEB in turn collisions: Collision avoided (Case3) and not avoided (Case4).

was 0.1 km/h and 10 km/h, respectively at t_E; and 7.1 km/h and 10 km/h, respectively, at the time of collision. In the reconstruction with AEB, the cyclist was continuously located outside the FOV because the cyclist approached the car from the side. As a result, the car could not stop to avoid the collision.

Fig. 17 shows the relationship between TTC_E and car velocity at t_E when the cyclist entered the intersection for three types of AEB sensors. Compared to perpendicular collisions, the vehicle velocity was relatively low and less than 30 km/h. Many collisions are not close to the brake performance line, which indicates that most collisions could be avoided if the AEB sensor detected the cyclist early. Among the 51 collisions, 29 collisions were avoided with 50° FOV. Fourteen (14) additional collisions were avoided by extending the FOV to 90°. A further 6 more collisions were avoided by extending the FOV to 360°. There was 1 collision that was not avoided though the car velocity was reduced with 360° FOV. In this case, the original collision point was the rear side of the car. Since the car stopped at the crosswalk using AEB and the cyclist was set to have same behavior with and without AEB, the cyclist therefore traveled along the original path and the collision point changed to the front side of the car. Furthermore, the AEB with 360° FOV did not activate for 1 collision. In this particular case, the cyclist suddenly entered the intersection at t_E, resulting in a small TTC, and the AEB did not start within DT 0.5 s.

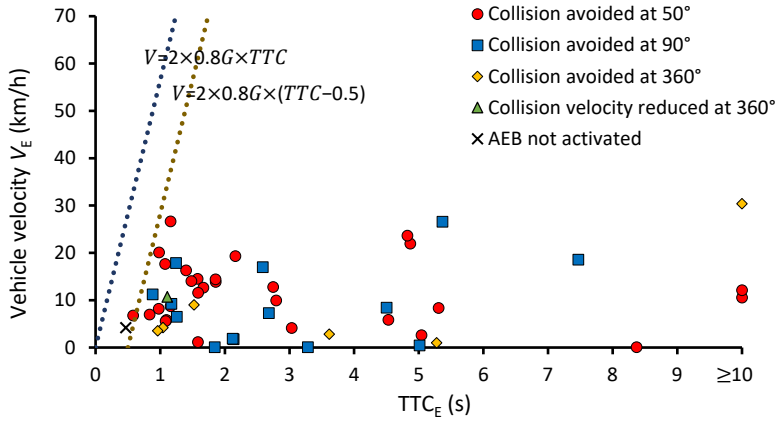

Fig. 17. Collision avoidance with TTC and vehicle velocity at t_E for various AEB FOVs and DT 0.5 s in left and right turn collisions.

The positions of the cyclists relative to the car at t_E for FOV 50°, 90° and 360° (DT 0.5 s) of AEB sensors in left and right turn collisions are shown in Fig. 18. The cyclists' positions were distributed wider than those of perpendicular collisions, and some cyclists were positioned around ±90° (x-axis). Irrespective of these wide distributions of the cyclists, many collisions could be avoided because of the low velocity of the cars. In the two collisions which were not avoided with FOV 360°, the cyclists appeared within 4 m from the car.

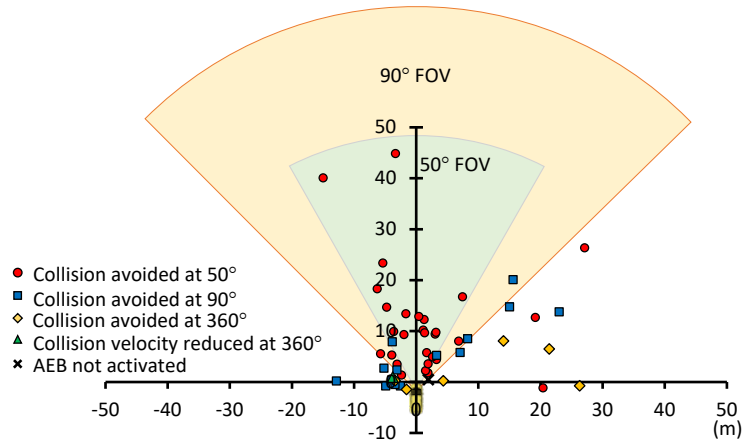

Fig. 18. Cyclist position relative to the car at t_E with collision avoidance for various AEB FOVs and DT 0.5 s in left and right turn collisions

Fig. 19 shows the collision avoidance with three types of AEB classified by the cyclist direction relative to the car. The effects of AEB on crash avoidance for the configurations of cyclist same direction was not large for both left and right turn collisions. This is because, when the cyclist travels in the same direction as the car, the cyclist approaches out of the FOV. Enlarging the FOV was effective in the configuration of cyclist traveling in the same

direction, and 90° FOV could avoid 70% of collisions. Finally, all collisions were avoided in the ideal AEB in the configuration of the cyclist traveling in the same direction.

Basically, when the cyclist approached from the opposite direction to the car's travel direction in either right or left turn, the AEB was effective since the cyclist entered the FOV earlier than that with the cyclist's traveling same direction. Enlarging the FOV was also effective for the case where cyclist approached in the opposite direction. Finally, there remained two collisions which could not be avoided using ideal AEB.

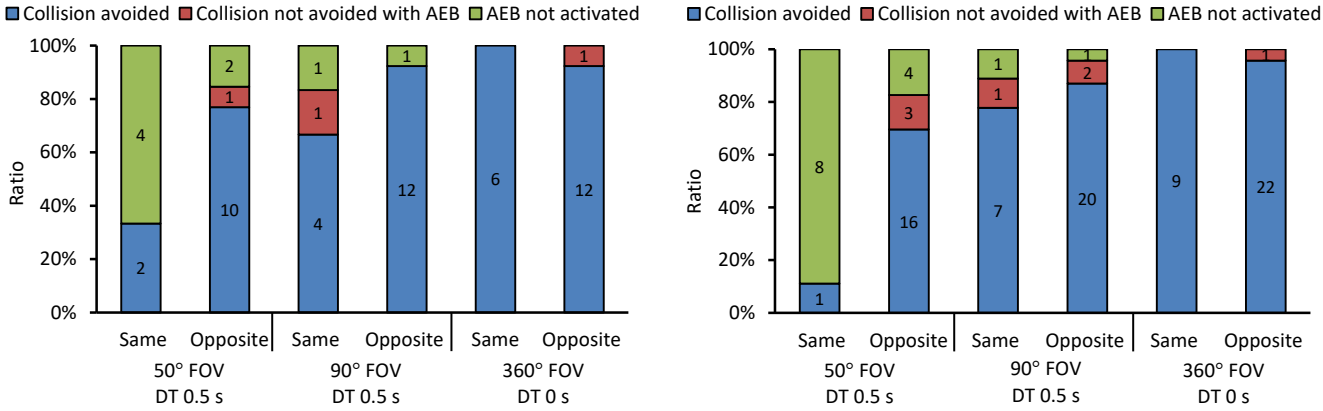

(a) Collision avoidance of right turn (N=19) (b) Collision avoidance of left turn (N=32)

Fig. 19. The ratio of AEB effectiveness in avoiding collisions in left and right turn collisions.

IV. DISCUSSION

In depth-accident data of car-to-pedestrian or car-to-cyclist collisions, the position of pedestrian or cyclist before impact include uncertainties. In contrast, video analysis has advantages that the pedestrian behavior can be observed [10, 11, 13, 14]. Particularly, cyclists have higher traveling velocities than pedestrians, and the cyclist behavior can be traced by analyzing the time sequence in the video. Using video, the cyclist trajectory can be plotted with time and it is observed that some cyclist trajectories are complicated (Fig. 7 & Fig. 8). Whereas, those plotted on the basis of in-depth data are relatively more simple [8]. In left and right turn collisions, it was observed from drive recorders that a car's velocity changed with time by braking before turning. The car velocity and acceleration can be obtained from the drive recorder's output signal. Furthermore, videos show the surrounding environment of the accident, which includes moving obstructions that prevented the cars' drivers from detecting the cyclists. From the video, pedestrians or cyclists can be observed as being obstructions (Fig. 6), while they are not listed as being obstructions in the depth-accident data [7].

Previous research using videos employed collision data [10,11] or near-miss incidents data, individually [13], whereas this study compared collision and near-miss incidents. It was revealed that the collisions occurred when the cyclist entered the area where the car deceleration of over 0.55 *G* was necessary for the car to stop (Fig. 9 & Fig. 10). This deceleration is less than the maximum deceleration of 1 *G* determined physically from the friction between the tire and the road since the time taken for the car to stop includes the drivers' reaction time and braking time. Two factors were identified that the car led to this area: drivers' braking delay and the sudden appearance of the cyclist. In the first type of collisions, TTC is more than 1 s, and can be avoided effectively by using AEB. In the second type of collisions, TTC is less than 1 s and is difficult to be avoided by using AEB. In left and right turn collisions, the car velocities tend to be low and only a few cases required 0.55 *G* to stop cars. Also, the left and right turn collisions occurred mainly due to the delay of drivers' perception.

In perpendicular collisions, the TTC was an important parameter in the collision occurrence, and enlarging the FOV can allow the AEB to detect the cyclist earlier. In left and right turn collisions, though the car velocity was low, the car direction changes and the FOV has a large influence on collision avoidance. In left and right turn collisions, when the cyclist traveled from the opposite direction of the car, the cyclist is included earlier in FOV, and these collisions could be avoidable. In contrast, when the cyclist traveled from the same direction of the car, the cyclist approached the car outside of the FOV 90° (Fig. 8(a) & (c)). Therefore, the AEB sensor did not detect the cyclists until the cyclist was positioned in front of the car. There is another factor that the ideal AEB did not activate in left and right turn collisions. In intersections, cyclists can enter from the pavement to the pedestrian crosswalk when the car is close to the pedestrian crosswalk. This situation can occur in the right turn opposite

direction and in the left turn same direction in right-hand drive traffic situations (Fig. 1(b)). It will be necessary to address for determining whether the cyclists enter the road or they stay in the pavement by the AEB algorithm.

The drawback of video analysis is that the number of collision data is not enough. The effectiveness of AEB based on in-depth accident data is expressed by the reduction of the number of injuries [3-9]. In our database, injury data are not recorded, and only collision occurrences could be examined. If the data were linked with police data or insurance data, a comprehensive analysis including the age and injury severity of the cyclists would be possible such as that done in the study by Kim et al. [10]. Besides, car impact velocities are low in the drive recorder data (Fig. 5(b)), which is comparable with velocities of all cyclist collision data in GDAS data [4]. Thus, the effectiveness of AEB in our study related to all collisions including no injuries. Rosén [5,6] showed that a large FOV could cover minor injuries to pedestrians in low impact velocities. In this study, enlarging FOV of AEB is more effective for collision avoidance. One reason may be the low velocity distributions of the car.

Though many cyclist collisions were avoided with ideal AEB, 20% of perpendicular collisions and 4% of left and right turn collisions were not avoided because of the cyclists' sudden appearances. These collisions might continue to occur in autonomous cars. Many of these cyclists' sudden appearances were related to the cyclists' behavior of violating traffic laws [14]. In addition, Räsänen and Summala [21] indicated that 66% of cyclists noticed the car before collisions, and 36% of cyclist took some behavior to avoid the collisions. As shown in Fig. 10, cyclist avoidance behavior was effective for collision avoidance.

V. LIMITATIONS

The data of taxi-cyclist collision were collected in Aichi prefecture. Since many of the data were collisions that occurred in city area, the dataset does not represent the full set of crash configurations in Japan. The accuracy of the drive recorder analyses and the accident reconstructions was not investigated. The model of virtual AEB system used in the PC-Crash reconstruction was simple and was assumed to work without errors to find cyclists, which can lead to the maximum effectiveness of an ideal AEB.

VI. CONCLUSIONS

In this study, based on videos from drive recorder, perpendicular and left and right turn car-to-cyclist collisions at intersections were analyzed and were reconstructed in PC-Crash while implementing a virtual AEB model. The results are summarized as follows:

1. From accident analysis of drive recorder, two factors leading to unavoidable collisions were identified: the driver's long reaction time and the cyclist's sudden appearance. In perpendicular collisions, both factors are important. In left and right turn collisions, the first factor is predominant as the car velocity is low.
2. In perpendicular collisions, many collisions resulting from the driver's long reaction time could be avoided by using AEB. The effectiveness of AEB can be increased by enlarging the sensor FOV angle. Nonetheless, even when using an ideal AEB (FOV 360 degrees and no braking time delay), some collisions where the cyclist appeared suddenly were possibly not be avoided.
3. In left and right turn collisions, enlarging the FOV was effective to avoid collisions by AEB especially for the case where the cyclist travels in the same direction as the car. It was difficult to avoid collisions by AEB where the cyclist entered the road from the pavement when the car was close to the cyclist.

VII. ACKNOWLEDGEMENT

This research was funded by a grant the Takata Foundation.

VIII. REFERENCES

[1] Rosén E, Stigson H, Sander U. Literature review of pedestrian fatality risk as a function of car impact speed. Accid Anal Prev. 2011;43:25-33.

[2] Tefft B. Impact speed and a pedestrian's risk of severe injury or death. Accid Anal Prev. 2013;50: 871-878.

[3] Rosén E, Källhammer J, Eriksson D, Nentwich M. Pedestrian injury mitigation by autonomous braking. Accid Anal Prev. 2010;42:1949-57.

[4] Rosén E. Autonomous emergency braking for vulnerable road users. IRCOBI Conference; Sep 11-13, 2013; Gothenburg, Sweden.

[5] Páez F, Furounes A, Badea A. Benefits assessment of autonomous emergency braking pedestrian systems based on real world accidents reconstruction, 24th International Technical Conference on the Enhanced Safety of Vehicles (ESV); June 8-11, 2015; Gothenburg, Sweden.

[6] Fredriksson R, Ranjbar A, Rosén E. Integrated bicyclist protection systems – potential of head injury reduction combining passive and active protection systems, 24th International Technical Conference on the Enhanced Safety of Vehicles (ESV); June 8-11, 2015; Gothenburg, Sweden.

[7] Op den Camp O, van Montfort S, Uittenbogaard J, Welten J. Cyclist target and test setup for evaluation of cyclist-autonomous emergency braking. International Journal of Automotive Technology. 2017;18(6):1085-1097.

[8] Lenard J, Welsh R, Danton R. Time-to-collision analysis of pedestrian and pedal-cycle accidents for the development of autonomous emergency braking systems. Accid Anal Prev. 2018;115:128-136.

[9] Barrow A, Edwards A, Khatry R, Cuerden R, Schneider A, Labenski V, Veh U, Casualty benefits of measures influencing head to windscreen area protection, IRCOBI Conference; Sep 12-14, 2018; Athens, Greece.

[10] Kim D, Sul J. Analysis of pedestrian accidents based on in-vehicle real accident videos, 23rd International Technical Conference on the Enhanced Safety of Vehicles (ESV); May 27-30, 2013; Seoul, Korea.

[11] Han Y, Li Q, He W, Mizuno K. Analysis of vulnerable road user kinematics before/during/after vehicle collisions based on video records. IRCOBI Conference; Sep 13–15, 2017; Antwerp, Belgium.

[12] Ito D, Hayakawa K, Kondo Y, Mizuno K et al. Difference between car-to-cyclist crash and near crash in a perpendicular crash configuration based on driving recorder analysis, Accid Anal Prev. 2018;117:1-9.

[13] Tsutsumi, S., Sato, K., Nagai, M. Analysis of vehicle accident involving bicycle at non-signalized intersection by near-crash incident database. Proceedings of the 3rd International Symposium on Future Active Safety Technology Toward Zero Traffic Accidents. 2015.

[14] Du E, Yang K, Jiang F et al. Pedestrian behavior analysis using 110-car naturalistic driving data in USA,23rd International Technical Conference on the Enhanced Safety of Vehicles (ESV); May 27-30, 2013; Seoul, Korea.

[15] Zhao Y, Ito D, Mizuno K. AEB effectiveness evaluation based on car-to-cyclist accident reconstructions using video of drive recorder. Traffic Inj Prev. 2019; 20(1): 100-106.

[16] Lindman M, Jonsson S, Jakobsson L, Karisson T, Gustafson D. Fredriksson A. Cyclist interacting with passenger cars; a study of real world crashes. IRCOBI conference, 2015.

[17] Kuehn M, Hummel T, Lang A. Cyclist-car accidents – their consequences for cyclists and typical accident scenarios. 24th International Technical Conference on the Enhanced Safety of Vehicles (ESV); June 8-11, 2015; Gothenburg, Sweden.

[18] Tanaka S, Teraoka E. Benefit estimation of active safety systems for crossing-pedestrian scenarios, FISITA World Automotive Congress; June 2-6, 2013; Maastricht, the Netherland.

[19] Euro NCAP. Test Protocol—AEB VRU Systems Version 2.0.2. 2017. Available from: https://www.euroncap.com/en/for-engineers/protocols/vulnerable-road-user-vru-protection/

[20] Seiniger P, Bartels O, Pastor C, Wisch M. An open simulation approach to identify chances and limitations for vulnerable road user (VRU) active safety. Traffic Inj Prev. 2013;14(Suppl. 1): S2–S12.

[21] Räsänen M., Summala H. Attention and expectation problems in bicycle–car collisions: an in-depth study, Accid Anal Prev. 1998;30(5):657-666.